Ceramics International 52 (2026) 4250–4258

Contents lists available at ScienceDirect

Ceramics International

journal homepage: www.elsevier.com/locate/ceramint

Mechanical behavior, numerical simulation, and cytotoxicity assessment of silicon nitride for dental application

Paula Cruz Mendes Silva [a,*], Pedro Araújo da Costa Ward [b], Patrick Lima Gomes [b], Thais Monteiro da Silva [a], Flávio Machado de Souza Carvalho [c], Daniel Perez Vieira [a], Dolores Ribeiro Ricci Lazar [a], Claudinei dos Santos [d], Cecilia Chaves Guedes-Silva [a]

[a] Instituto de Pesquisas Energéticas e Nucleares, Comissão Nacional de Energia Nuclear, Avenida Prof. Lineu Prestes, 2242, 05508-000, São Paulo-SP, Brazil
[b] Universidade Federal Fluminense - Escola de Engenharia Industrial Metalúrgica de Volta Redonda – UFF/EEIMVR, Avenida dos Trabalhadores,420, Vila Santa Cecília, 27.255-125, Volta Redonda-RJ, Brazil
[c] Universidade de São Paulo, Instituto de Geociências, Rua do Lago, 562, 05508-080, São Paulo-SP, Brazil
[d] Universidade do Estado do Rio de Janeiro - Faculdade de Tecnologia de Resende UERJ/FAT, Rodovia Presidente Dutra, Km 298, 27.537-000, Resende-RJ, Brazil

ARTICLE INFO

Handling Editor: Dr P. Vincenzini

Keywords:
Dental implants
Silicon nitride ceramics
Numerical simulation
Finite element method

ABSTRACT

This study aimed to evaluate the potential of silicon nitride as a material for dental implants, focusing on its key properties, including high mechanical strength, chemical compatibility, excellent imaging characteristics, and antibacterial activity. Therefore, samples of silicon nitride ceramics with SiO_2 and CaO as additives were pressureless sintered at 1800 °C for 1 h, and then characterized in terms of microstructure, mechanical properties, and biological behavior. Additionally, the mechanical behavior of a Si_3N_4 implant under masticatory loads was simulated using the Mohr-Coulomb criterion to assess risk of failure. The results showed that the prepared silicon nitride ceramic was non-cytotoxic and exhibited density, Vickers hardness, fracture toughness, compressive strength and Young's modulus of 3.10 ± 0.01 g/cm^3, 12.17 ± 0.35 GPa, 7.54 ± 0.78 MPa m$^{1/2}$, 1497.42 ± 74.06 MPa, of 211.23 ± 63.81 GPa, respectively. It demonstrates that the material is a promising ceramic for dental implants, especially when compared to conventional biomaterials typically used in implant applications. Supported by the experimental results, numerical simulations using the finite element method suggested that the Si_3N_4-based ceramic developed in this work was able of withstanding masticatory loads of up to 400 N (under normal, compressive loads) and 350 N (under occlusal loads), without risk of failure, within the simulation parameters adopted in this study.

1. Introduction

Many materials have emerged as key solutions in orthopedic and dentistry to address health issues resulting from injuries, fractures, and degenerative diseases. These materials play a crucial role in applications such as prosthetics, implants, and bone grafting [1–3]. Titanium and its alloys remain the most used materials for dental implants due to its biocompatibility and strength and durability. Despite their widespread use, the high prevalence of bacterial-origin peri-implant diseases characterized by inflammation of the surrounding mucosa and, in some cases, progressive loss of supporting bone, often requires the implant retrieved [4,5].

The corrosion products of titanium tend to increase the implant failure rate and immunologically mediated reactions in the surrounding tissues due to the accumulation of metal particles [5,6]. Additionally, dental clinics are experiencing a daily increase in patient demand for metal-free dental rehabilitation that provides superior aesthetic results [4,5]. Metallic implants can disturb the distribution of light reflected through the crown, leading to reduced translucency. A grayish halo can also be created in the gingival margin of the implant as a result of a thinner gingiva or even bone loss [3]. Several factors can help to minimize bone loss and address the associated issues, with customized implants being one of them. By being tailored to the patient's specific needs, customized implants can reduce the risk, but cannot fully eliminate the possibility of failure [7]. To overcome the limitations of the grayish halo, patient rejection of metal implants, and the problem of corrosion products, metal-free dental implants have been introduced to the market, with ceramic implants already in use. Zirconia is the main

* Corresponding author.
E-mail address: paula.cmendes@usp.br (P.C.M. Silva).

https://doi.org/10.1016/j.ceramint.2025.12.177
Received 13 December 2024; Received in revised form 10 December 2025; Accepted 11 December 2025
Available online 16 December 2025

ceramic material owing to biocompatibility, strength, corrosion resistance and aesthetic which makes it particularly suitable for visible areas, such as the front teeth, where appearance is essential [4,5,8]. The most significant advantage of zirconia is the crack propagation resistance attributed to the volume expansion of grains during the tetragonal to monoclinic ($t \rightarrow m$ ZrO_2) phase transformation. However, this transformation can also lead to implant failure due to the stress from repeated loading and environmental exposure to body fluids, such as blood or saliva. Moreover, the high radiopacity of zirconia makes it challenging to visualize the surrounding bone tissue in postoperative imaging exams [3].

New ceramic materials for dental applications have been extensively investigated, with silicon nitride (Si_3N_4) emerging as a promising candidate [9,10]. This potential is largely due to prior studies on its use in high-performance technical applications, such as cutting tools, bearings, and engine components, owing to its exceptional wear resistance, thermal shock tolerance, high mechanical strength, and relatively high fracture toughness [11,12,13,14]. Building on these properties, silicon nitride has been explored for biomedical applications, including hip and knee endoprosthetic implants, as well as plates and pins for bone fixation [6,10]. This material has been shown to not induce inflammatory reactions when implanted in animals. While the remodeling process is similar to that of titanium, it is more pronounced around silicon nitride. Furthermore, bone formation on the implant surface within the marrow cavity of rabbit tibias highlights the osteoconductive properties of silicon nitride. Since 2008, silicon nitride has been utilized in fusion cages for cervical and thoracolumbar spinal arthrodesis. In the dense form, silicon nitride presents a high Young's modulus in comparison to metallic and polymeric implants. However, it can confer clinical benefits in its porous form.

The potential of silicon nitride for dental applications is attributed to its osseointegration, superior tribological properties as well as moderate radiolucency. The high mechanical properties can allow the material to withstand the repetitive forces faced during mastication. This last characteristic ensures good implant compatibility with important medical imaging techniques, including X-rays, magnetic resonance imaging, and computed tomography [6,9,10,12,13]. Although long-term data on silicon nitride dental implants is still limited, early studies suggest they have the potential to last as long as titanium implants, primarily due to their resistance to wear, corrosion, and their excellent strength-to-weight ratio. Also, its inherent bacteriostatic properties help prevent peri-implantis, reduce the risk of implant loss and discomfort during the healing process [4]. Silicon nitride exhibits superior performance against bacterial adhesion and biofilm formation compared to other implant materials like titanium alloys. For example, Wu et al. [15] demonstrated that silicon nitride significantly reduces colony-forming units (CFUs) of both *Staphylococcus aureus* and *Escherichia coli*, with its chemical properties playing a crucial role in its ability to effectively resist bacterial colonization. This unique combination of features is not present in titanium and zirconia, thereby explaining the increasing interest in silicon nitride as dental implants although bone grafts may be necessary particularly in older individuals to provide mechanical support and stimulate bone regeneration, similarly to other biomaterials [16].

The superior biological behavior of silicon nitride ceramics over zirconia and titanium was well demonstrated by Wu et al. [15]. The authors observed that human bone mesenchymal stem cells (hBMSCs) adhered and proliferated more effectively on polished Si_3N_4 compared to titanium and zirconia and noted its improved osteogenic activities and superior antibacterial properties. To further enhance the biological response of biomedical zirconia, Marin et al. [17] applied a Si_3N_4 coating to zirconia substrates. The results revealed that, compared to uncoated zirconia, the silicon nitride coating significantly improved cellular adhesion and promoted bone tissue formation, with higher levels of maturity and overall better quality. Moreover, experiments with SaOS-2 cells performed by Pezzotti*et al.* [18] showed that a Si_3N_4 coating significantly enhanced osteogenesis, when deposited on zirconia-toughened alumina (ZTA). In a related study, Ozodogan et al. [9] evaluated porous Si_3N_4 aiming use in all-ceramic restorations, and its performance was compared to commercial ZrO_2 ceramics. The findings show that Si_3N_4 exhibited excellent mechanical properties, including a flexural strength of 418 MPa and a hardness of 10.9 GPa. Through controlled porosity, ceramics with a suitable color shade for restorative applications were achieved. The radiolucent properties of Si_3N_4 also allow clear imaging of both the restorations and surrounding tissues using plain radiography.

In recent years, studies on numerical simulations using the finite element method (FEM) to evaluate the mechanical properties of ceramic materials have received great attention. Numerical simulation of the mechanical properties of ceramic dental implants has been studied in different studies focusing on ceramics based on yttria-stabilized zirconia or ceramic composites containing zirconia in their composition [19–21]. This particular interest in simulations of zirconia implants is justified by the existence of commercial products already available in the dental market, in addition to the intrinsic characteristics of tetragonal zirconia, such as excellent aesthetics, flexural strength and fracture toughness. Numerical simulations of properties of silicon nitride based ceramics have been published focusing on phenomena related to the liquid phase sintering process [22], or mechanical properties in usual applications, such as structural ceramics and as machining tools [23,24]. Investigations regarding their fracture toughness and respective fracture mechanisms have also been performed [25]. Although researches on the numerical simulation of the mechanical behavior of silicon nitride implants are limited, a study simulating a Si_3N_4 prototype for an osteofixation system demonstrated good mechanical stability for osteosynthesis of the frontal bone [26].

The literature indicates that the microstructure and mechanical properties of silicon nitride ceramics using CaO and SiO_2 as sintering aids enhances bioactivity and improve bone tissue interaction due to the formation of a glassy phase [27,28]. A slight dissolution of the glass phase may occur in physiological fluid on the material surface, but the released cations could be beneficial to new bone formation. This highlights the importance of selecting appropriate sintering additives that form the glass phase [29]. In view of this information, the objective of the study was to develop and characterize a ceramic composition based on silicon nitride (Si_3N_4) with mechanical and biological properties suitable for use as a dental implant. Moreover, it was performed the simulation of the mechanical behavior of a Si_3N_4 implant geometry subjected to different masticatory loads. For this purpose, the Mohr-Coulomb criterion was used to determine the risk of failure of this implant as a function of masticatory loads.

2. Experimental procedure

2.1. Sample preparation

As starting materials, α-Si_3N_4 (Höganäs M11, >90 % α-Si_3N_4), SiO_2 (Sigma-Aldrich, quartz, 99.9 % purity), and $CaCO_3$ (Vetec, 97 % purity) were used. The powders were dosed to prepare a composition (SNSC code) containing 80 wt % Si_3N_4,10 wt % SiO_2, and 10 wt % CaO, which were milled in a ball mill for 24 h, using isopropyl alcohol as liquid medium. After milling, the slurry was dried in a rotary evaporator at 70 °C and green compacts were formed using uniaxial (30 MPa) and cold isostatic pressing (200 MPa), respectively. The green compacts were sintered in a graphite resistance furnace (Thermal Technology) at 1800 °C for 1 h, using a heating rate of 10 °C/min, in a controlled nitrogen atmosphere.

2.2. Structural characterization

The sintered samples were evaluated for density and apparent porosity using the Archimedes' method, with measurements taken from

five specimens. The secondary crystalline phases and the α→β transformation were analyzed by X-ray diffraction with Cu-Kα radiation (XRD, Brucker D8). The grain shape and distribution, as well as the porosity present in the samples, were evaluated using scanning electron microscopy (FEG-SEM, JSM-IT700HR) of polished samples etched with sodium tetraborate.

2.3. Mechanical properties

Vickers hardness and indentation fracture toughness tests were performed using a hardness tester (Buehler VH1150), applying a 98 N load for 15 s on a polished surface, with eight indentations made. The diagonals and cracks length were measured using optical microscopy. Therefore, Vickers hardness was determined using Equation (1) [30].

$$H_v = \frac{1.8544xP}{a^2} \quad (1)$$

"*P*" and "*a*" parameters are the applied load and indent diagonals, respectively. The fracture toughness values were calculated using Equation (2) provided by Asntis et al. [31], as follows.

$$K_{Ic} = 0.016x\left(\frac{E}{H_v}\right)^{\frac{1}{2}} x\frac{P}{c^{\frac{3}{2}}} \quad (2)$$

Herein, "K_{IC}" is the fracture toughness, "*c*" the crack length, "H_V" the hardness and "*E*" Young's modulus.

The Young's modulus (E) was estimated using nanoindentation tests with a Shimadzu DUH-211S ultra-microhardness tester (Japan), equipped with a diamond Berkovich indenter. In this characterization step, 15 indentation measurements were performed, using an indentation load of 1960 mN, with maximum penetration depth of 10 μm. Data analysis was conducted following the Oliver and Pharr method [32,33]. Compressive strength (10 specimens) was measured using an Instron 4400 universal testing machine, with a loading speed of 4.0 mm/min.

2.4. Cytotoxicity tests

Cell culture: Murine fibroblasts, NIH/3T3 cell line (ATCC CRL-1658), were cultured in 5 mL of RPMI 1640 medium, pH 7.4 (Gibco, Grand Island, USA), supplemented with 10 % fetal bovine serum (Cultilab), 2 g/L sodium bicarbonate ($NaHCO_3$, Sigma-Aldrich), and a 1 % solution of penicillin and streptomycin (10,000 U/10,000 μg/mL, Gibco) in sterile plastic cell culture flasks with 25 cm^2 culture area (Corning), kept in incubators with controlled atmosphere and temperature (5 % CO_2, 37 °C), until confluence was approximately 60–70 %, as estimated by visual inspection, with medium changes every 48 h. Subsequently, the culture medium was removed; the adherent cells were washed with sterile phosphate-buffered saline (PBS) at 37 °C and treated with a 0.25 % trypsin solution with 0.02 % disodium EDTA (Sigma-Aldrich) to obtain completely dissociated cell suspensions. Only viable fractions, identified by the lack of trypan blue dye (0.4 %, Life Technologies) incorporation, were considered for subculture or experimentation.

Ceramic extracts: Specimens of the ceramics were immersed in culture medium for 24 h at 37 °C to produce extracts corresponding to 1500 mg/mL. After, the extracts were sterilized by filtration (0.22 μm) and diluted in culture medium to obtain the experimental dilutions.

Cytotoxicity/Cell Viability Assay: To determine the toxic and non-toxic concentrations of the ceramic extracts, cells were trypsinized and seeded (10,000 cells/well, 100 μL/well) in a 96-well plate and allowed to adhere for 24 h in an incubator as described. Then, the medium was removed, and 100 μL of control solutions and ceramic extracts were added in quadruplicates and left in culture for the subsequent 24 h. Positive control wells were treated with dimethyl sulfoxide (DMSO, Sigma-Aldrich) at 10 % and diluted in a culture medium. Negative controls received NaCl at a final concentration of 0.045 %. Additionally, cells cultured in RPMI 1640 medium without any added compounds were used as the basal control (CC). After 24 h of incubation, the culture medium was removed, and the cells were washed with 100 μL of PBS (37 °C) to remove any test substance residues. An MTS solution (2 mg/mL PBS, Promega) and PMS (0.92 mg/mL PBS, CAS 299-11-6, Sigma-Aldrich) in medium were added (100 μL/well). Absorbance (490 nm) was measured using a microplate reader (Multiskan EX, Labsystems) 2 h after incubation in the incubator.

Result analysis: The cell viability of each test group was calculated based on the control CC (% of controls). Cytotoxicity values for each sample and control were compared to the basal controls (CC) using one-way analysis of variance (One-way ANOVA), and differences between groups were evaluated using the Bonferroni post-test.

3. Finite element modelling

3.1. Implant geometries and mandible model

In this study, it was used a geometric model referring to a commercial implant [34] with 9.8 mm in height and diameter ranging from 4.8 mm (implant head) to 4.1 mm (thread region), with a thread pitch of 0.8 mm. Moreover, the implant was assumed to be anchored in the region of the human mandible referring to the positioning of the second-molar tooth (SM). Fig. 1 shows details of the design of the implant and the mandible, indicating the implant positioning. It was considered a slice of the mandible of an adult male aged 40 years old closer to the implant region.

During the creation of the 3D model, it is possible to choose to use tetrahedral or hexahedral elements in numerical simulations. Tetrahedral elements were used in this work due to the geometric complexity of the model. In regions with irregular surfaces or small details, the tetrahedral mesh usually shows better adaptability and generates a more robust filling without the need for geometric simplification. Furthermore, it allows for faster and more stable mesh generation for numerical simulations, compared to hexahedral elements, which generally require more regular geometries to maintain good quality. They allow automatic meshing algorithms that can handle complex geometries as described by Schneider et al. [35].

3.2. Model assembly and finite element meshing

For all finite element simulations, it was used the commercial software ABAQUS/Standard version 6.9, in a Xeon 5690 3.47 GHz dual-processor, 24-core, 32 Gb RAM workstation. As a strategy to save CPU time, simplified assembly finite element models were proposed during the pre- (meshing) and post-processing steps. Fig. 2a illustrates the complete assembly of the second-molar (SM) implant in the mandible. Highlighted in this figure, the brown regions correspond to the simplified assembly models. The finite element analysis comprises two models representing the dental implant region (second-molar) and the implant base material (silicon nitride). The simplified assembly models were discretized using 4-nodes 1st-order tetrahedral elements that is, the condition of the implant bonded to the mandible, denoted as C3D4 according to ABAQUS terminology. The mesh size of the mandible was set to 0.5 mm, while a smaller size of 0.25 mm was adopted in the dental implant elements. The element sizes of 0.25 mm and 0.5 mm were defined based on the level of detail required in critical regions of the model. The smaller size was applied where there were high stress gradients, in this case in the implant. The larger size was adopted in regions of less impact, i.e., in the mandible, to optimize processing time. These values were defined according to the implant dimensions and tested numerically until the values converged and there was no further need for mesh refinement. Moreover, it was the mesh size which resulted in the best value to balance processing time and accurate result, as determined by previous analysis [20]. Fig. 2b illustrates details of the finite element mesh generated using the ABAQUS CAE pre-processor for the second-molar (SM) region, the details of which are summarized in

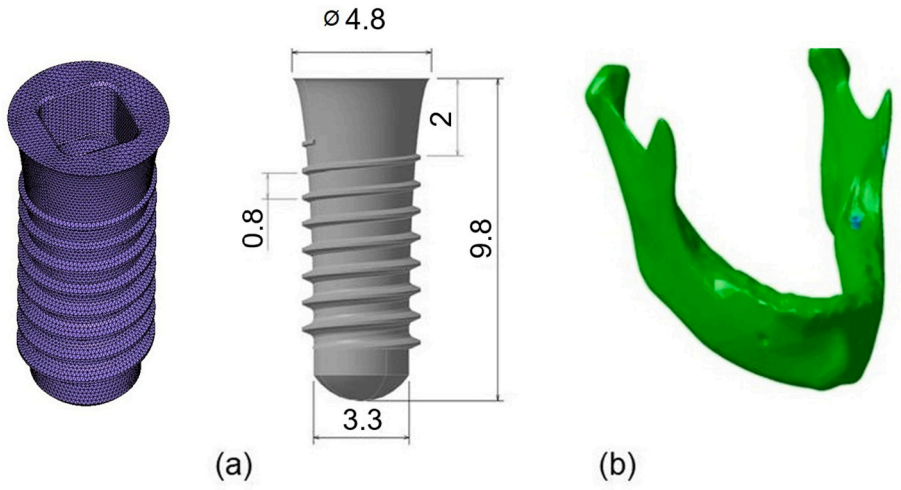

Fig. 1. (a) Implant geometry (mm) used in numerical simulations in second-molar (SM); (b) Geometry of a typical human mandible with SM implant position.

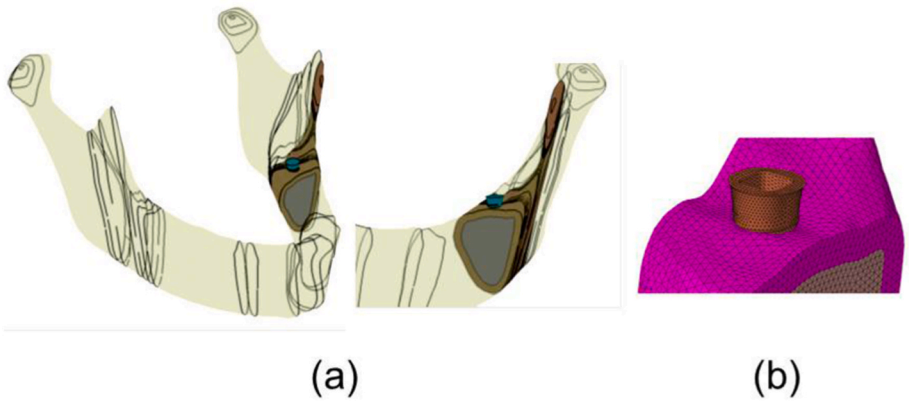

Fig. 2. (a) Full assembled and simplified geometrical models of second-molar dental implant based on Si_3N_4 ceramic in mandible model; b) Finite element meshing generated for second-molar (SM) region.

Table 1
Finite element meshing data of the models used for the third-molar mandible-region (First-order tetrahedral elements (4-node).

Region	Elements	Nodes
Si_3N_4 Implant	29,857	135,005
Cortical bone	23,798	103,006
Spongy bone	34,518	164,281

Table 1.

3.3. Mechanical behavior and failure risk

As a premise of the finite element analyses, the mechanical properties of the ceramic implants and bone materials were assumed to be isotropic, as described by Hooke's generalized linear isotropic theory. The assumed Poisson's ratio was 0.28, typical for silicon nitride ceramics [36]. The Young's modulus and compressive strength adopted in the finite element simulations are listed in Table 2. In addition, two types of bone properties were considered in the mandible due to their different mechanical properties. In Fig. 3, the brown region represents the cortical bone, while the central grey region is the spongy bone. A tethered contact was assumed between the cortical and cancellous bone surfaces and the corresponding implant surfaces.

Table 2
Elastic material properties of the finite element models [35–37].

Material	E (MPa)	ν
Si_3N_4-SiO_2-CaO (80:10:10 wt%)	211,000 (Current work)	0.28 Ref.[36]
Cortical bone [38]	15,000	0.30
Spongy bone [38]	1,370	0.30

A prediction of the in-service failure risk of Si_3N_4 implants could be estimated using the Mohr-Coulomb isotropic yield criterion, which was defined in Equation (3) [37]:

$$\left(\frac{\sigma_1}{\sigma_{ut}}+\frac{\sigma_3}{\sigma_{uc}}\right)\leq 1 \tag{3}$$

In this Equation, values of σ_{ut} and σ_{uc} are the ultimate ceramic strength in uniaxial tension ($\sigma_{ut}=280$ MPa) [38] and compression ($\sigma_{uc}=1497.4$ MPa, see Table 3), respectively, whereas σ_1 and σ_3 stand for the maxima and minima values of the principal stresses.

In the finite element code ABAQUS, the risk of failure analysis was performed as a post-processing step from the principal stress components values (σ_1,σ_2,σ_3) with the corresponding mechanical properties of the implant materials, extracted from the experimental results cited in the following section. The failure risk of the implant material was verified as the left-hand sides of Equation (3) approach unity.

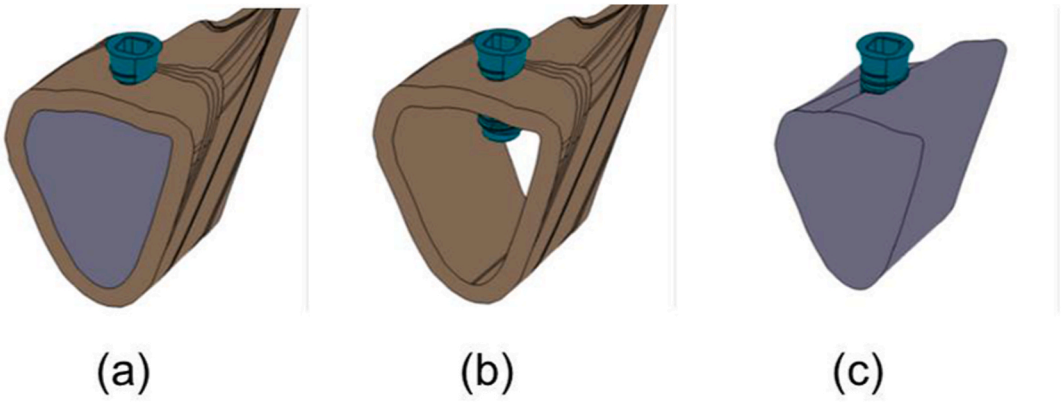

Fig. 3. Geometries of the finite element model for the second-molar (SM): (a) complete model, (b) implant and cortical bone, and (c) implant and spongy bone.

Table 3
Density and mechanical properties of prepared based Si_3N_4 sample (SNSC) and biomaterials from the literature [40b, 41–44].

Properties	SNSC (current work)	Al_2O_3	ZTA	Y-TZP	Ti alloy	PEEK	Cortical bone
Density (g/cm^3)	3.10 ± 0.01	3.97	4.37	6.10	4.43	1.29	1.85
Hardness (H_V)	12.17 ± 0.35	19.1	19.1	12.5	3.40	0.40	0.50
Fracture toughness (MPa m$^{1/2}$)	7.54 ± 0.78	4.50	5.70	10.5	75.0	2.00–8.00	2.2–6.4
Young's modulus (GPa)	211.23 ± 63.81	435	350	210	110	4	8.0–12.0
Compressive strength (MPa)	1497.42 ± 74.06	2500	4300	2200	958	135	160

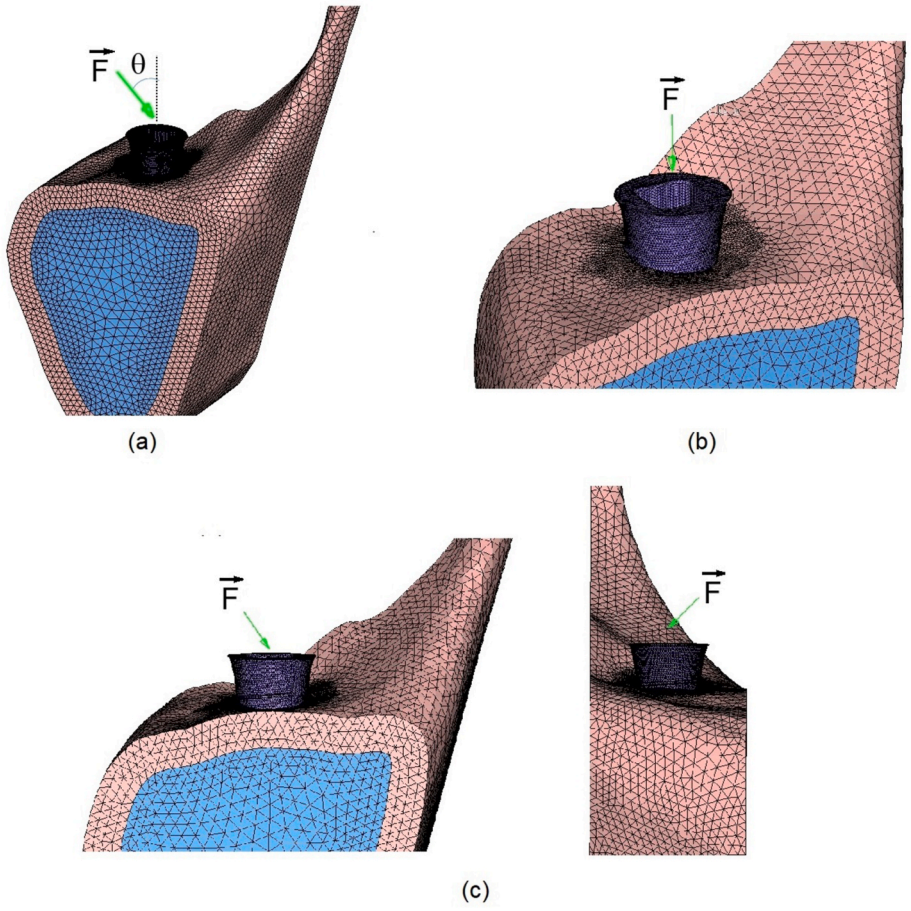

Fig. 4. (a) Simplified finite element models of the mandible in implant region (F = Load applied: 50N to 500 N): b) Displacement boundary conditions applied to the proposed finite element models (θ = 90°), c) Loads applied at θ = 45° and rotating about the implant axis.

3.4. Loading and boundary conditions

In the finite element model of the second-molar region, represented in Fig. 4, masticatory loads of 50 N–400 N were applied using load increments of 50 N. In addition, in the simulations a loading condition containing an angle of 45° or 90° in relation to the longitudinal axis of the implant corresponding to occlusal masticatory loads on the upper surface of the implant was applied. Fig. 4b and c shows the adopted displacement boundary conditions, which are applied to the externally sliced surfaces of the second-molar and central incisor finite element models by setting to zero the Cartesian (X, Y, Z) displacements in their corresponding regions. The boundary condition adopted fixed support without degrees of freedom on the sectioned faces in the mandible. It was adopted to simplify the computational processing, preventing any unrealistic movement or deformation at the sectioned interfaces [20]. Moreover, it was created TIE-type contact, that is, the condition of the implant "glued" to the mandible, without degrees of freedom and without the existence of friction.

4. Results and discussion

4.1. Microstructure and mechanical properties of sintered samples

Fig. 5a presents the XRD analysis of the Si_3N_4 ceramic, revealing the presence of β-Si_3N_4 and wollastonite as crystalline phases. This indicates that the α-Si_3N_4 initially present in the raw powder was completely transformed into β-Si_3N_4 during sintering at 1800 °C for 1 h. It is well known that silicon nitride is difficult to densify through solid-state diffusion due to its strong covalent bonding and the inherently low diffusivity of its constituent elements. For this reason, Si_3N_4 ceramics are typically consolidated by liquid-phase sintering, in which sintering additives react with the native SiO_2 layer on Si_3N_4 particles to form a liquid phase at the sintering temperature. This liquid phase enhances particle rearrangement and mass transport, enabling densification. During this process, the α-Si_3N_4 particles dissolve into the liquid phase and subsequently reprecipitate as β-Si_3N_4, following the classical three-stage mechanism of rearrangement–dissolution–precipitation [39]. The XRD results obtained in this study confirm that the sintering additives, i.e. SiO_2 and CaO, were effective in promoting the densification of silicon nitride through this mechanism. Additionally, wollastonite was formed by crystallization of the liquid phase during cooling from the sintering temperature. The presence of secondary phase at grain boundaries is typical of liquid-phase-sintered Si_3N_4 ceramics and can influence both the mechanical behavior and the long-term stability of the material [40a, 40b].

The rod-like β-Si_3N_4 grains are clearly visible in the SEM image shown in Fig. 5b, which displays the surface micrograph the silicon nitride ceramic. The β-Si_3N_4 phase exhibits superior mechanical properties compared to the α phase, making the ceramic suitable for structural biomedical applications such as dental implants.

The properties of the silicon nitride ceramics, compared to the average properties of titanium alloy, alumina ceramics, PEEK and cortical bone, are summarized in Table 3 [40b,41–44]. The sample achieved an apparent density of 3.10 g/cm^3 which corresponds to a relative density of 95.3 %, calculated using a value of 3.25 g/cm^3 estimated by the rule of mixtures. This result confirms that the additives combination was effective in promoting the liquid-phase sintering of the material, favoring its strength and reliability, which is particularly advantageous for dental applications, where long-term stability is essential.

Another critical characteristic observed in the studied sample, essential for ensuring long-term stability and the overall success of the implant, was the Young's modulus of 211.23 GPa. It is a low value for silicon nitride ceramics, which typically exhibit a Young's modulus of around 300 GPa in their completely dense form [44]. The reduced modulus is attributed to the intergranular secondary phase present in the sample. On the other hand, the measured hardness of 12.17 GPa is a promising result for dental implant applications, since it is comparable to Y-TZP, a well-established and clinically successful ceramic in dentistry. In addition, this value is lower than those found for Al_2O_3 and ZTA (Table 3). For implants, hardness plays a minor role in masticatory contact, as the implant itself does not undergo occlusal wear - this function is performed by the prosthetic crown. Instead, hardness is primarily important for ensuring structural strength, mechanical stability during placement, and long-term durability in the biological environment [45].

The fracture toughness of the studied ceramic was relatively high (7.54 MPa m$^{1/2}$), a key metric to preview ceramics resistance to crack propagation. Typically, the fracture toughness of silicon nitride ceramics falls within the range of 5.0–7.0 MPa m$^{1/2}$ [10], as a function of the processing methods, additives, phase composition and testing techniques used. The fracture toughness of silicon nitride is influenced by its grain morphology, i.e., elongated β-grains in a fine-grained matrix enhance fracture toughness. Notably, the measured value exceeds that of other biomaterials such as alumina, alumina–zirconia composites, and PEEK, as well as the performance requirements for biological implants.

The high compressive resistance achieved by silicon nitride (1497.42 MPa) ensures that this material can maintain structural integrity over time, reducing the risk of fractures from chewing and

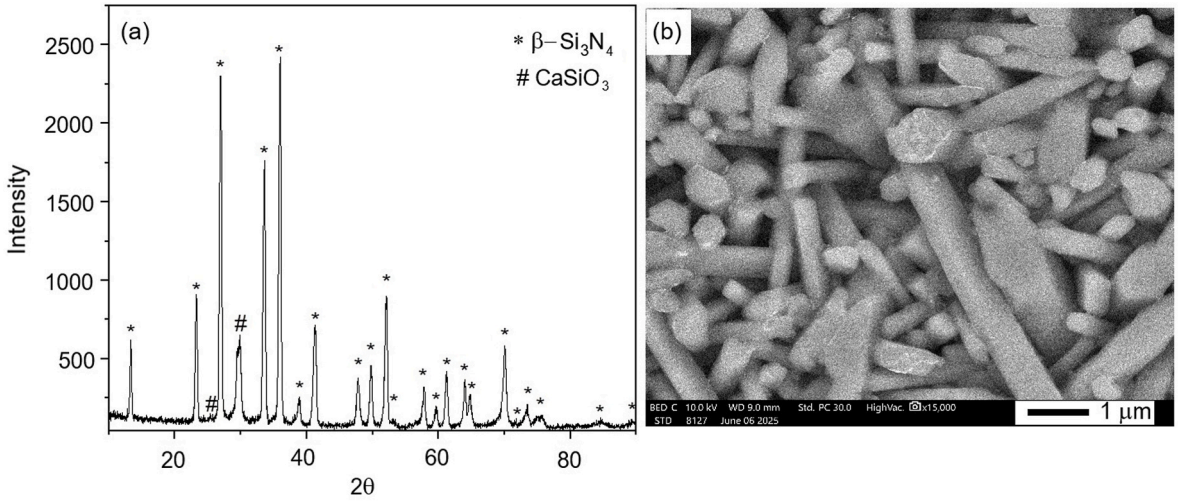

Fig. 5. (a) XRD spectrum and (b) SEM image of sintered SNSC sample.

biting that could compromise both aesthetics and function. The global evaluation of Table 3 data confirms the promising behavior of silicon nitride based ceramic as a dental material.

4.2. Cytotoxicity evaluation

Fig. 6 illustrates the effect of various extract concentrations (1–1500 mg/mL) of the ceramic on cell viability. The cytotoxicity tests showed high viability in all cultures exposed to the ceramic extracts, with cell viability remaining above 90 % at all extract concentrations. There were no significant differences in cell viability compared to the negative control.

Using "reference-man" calculations, which assume an adult male has 5.3 L of blood [46], SNSC ceramic exhibited no significant cytotoxicity at concentrations below 22 mg/mL, corresponding to an implant weight of approximately 121.9 g. This amount is far beyond what would be used in clinical practice, indicating that the ceramic is non-toxic under conditions relevant for patient applications. These results support the biocompatibility of the material and suggest a wide safety margin for its use in implants.

4.3. Numerical predictions

As previously mentioned, the corresponding SM Si_3N_4 implant principal stress values were determined for the adopted failure yield criterion: Mohr-Coulomb (MC). The results are presented in masticatory loads between 50 N and 400 N, and in two distinct groups: a) Application of uniaxial loads to the axis of the ceramic implant under normal conditions; b) Application of occlusal loads at an angle of 45° in relation to the axis of the implant, and in four different rotation positions of this load in relation to the axis of the implant. Then, the numerical predictions of the risk of failure are presented for Si_3N_4 implants under loading condition at every 50 N.

The results of the numerical simulation performed on the Si_3N_4 implant prototype, as a function of the applied load and the angle of application of this load, are presented in Figures S1 and S2 and detailed in Table 4, as a function of the risk of failure.

It can be seen in Fig. S1 that, regardless of the value of the masticatory load applied (100N, 200N, 300N, 350N and 400N), the critical regions of stress in the ceramic material are located in the region of the head of the implant screw. Despite this, in all the numerical simulations proposed in this study, under normal masticatory (90°) loads, no values represented risk of failure for the implant, when implanted in the region of the second-molar in the human mandible, presenting reliable MC values between 0.0949 (MC-50N) and 0.3797 (MC-400N).

From Fig. S2, in which four different applications of occlusal loads at 45° to the implant axis were simulated, it can be observed that the stress levels simulated by finite elements are still satisfactory, with MC values < 1, in simulations of masticatory loads of up to 300 N, indicating the full reliability of the implants. When the simulations were performed with loads of 350 N, slightly higher MC values were observed (MC between 1.029 and 1.095), which is the simulated limit masticatory load for the application of these implants, considering a safety margin for the risk of failure. However, in some specific rotation positions in occlusal loads, the implant head suffers a little more with the masticatory forces applied. This behavior is justified by the difference in implant anchorage in relation to the anatomical mandible, as illustrated in Fig. 4c. Even so, using the proposed implant geometry and its positioning within the mandible, the application of occlusal masticatory loads does not pose a risk to the integrity of the implant. The transition from satisfactory performance at 300 N to critical MC values (1.029–1.095) at 350 N under 45° oblique loading represents a clinically significant finding that aligns with biomechanical principles documented in the literature.

Oblique loading consistently produces substantially higher stress intensities in implants, abutments, and peri-implant cortical bone compared to vertical loading [4,5]. Studies have identified oblique force directions as primary risk factors in implant biomechanics [47]. Has and Orbak [48] reported significant stress increases under oblique loading and emphasized oblique force direction as a critical consideration in atrophic mandibles. Comparative FEA studies of ceramic versus titanium implants have documented higher stresses under oblique loading, with stress concentrations occurring in similar implant regions regardless of material [49]. Loads under oblique conditions are particularly relevant for clinical practice, as this represents parafunctional forces that may occur during bruxism or clenching episodes. However, recent studies have shown that occlusal splints can effectively reduce stresses for oblique loading in ceramic implant systems, suggesting potential clinical interventions for patients at risk of excessive loading [50]. Moreover, key implant design features, such as size, thread shape, platform configuration, and surface texture, directly affect how stress is distributed to surrounding bone. Larger diameters help reduce stress, especially in softer bone, while rough surfaces enhance early integration by supporting bone cell activity [48].

Hence, the results shown in Table 4 clarify that, in all cases studied, the Mohr-Coulomb ratio values were less than unity (MC < 1), indicating that the material does not present a risk of failure during the application of the types of masticatory loads proposed in the study. It is important to emphasize that the present investigation serves as a reference, since it is the first demonstration of the mechanical feasibility of silicon nitride dental implants, relating experimental results and numerical simulations. Hence, the search for improvements in mechanical properties combined with propitious biological behaviour is essential to ensure a high level of reliability for silicon nitride in dental applications.

5. Conclusions

The sintered Si_3N_4 ceramics, containing 10 wt% SiO_2 and 10 wt% CaO as additives presented a typical microstructure with elongated

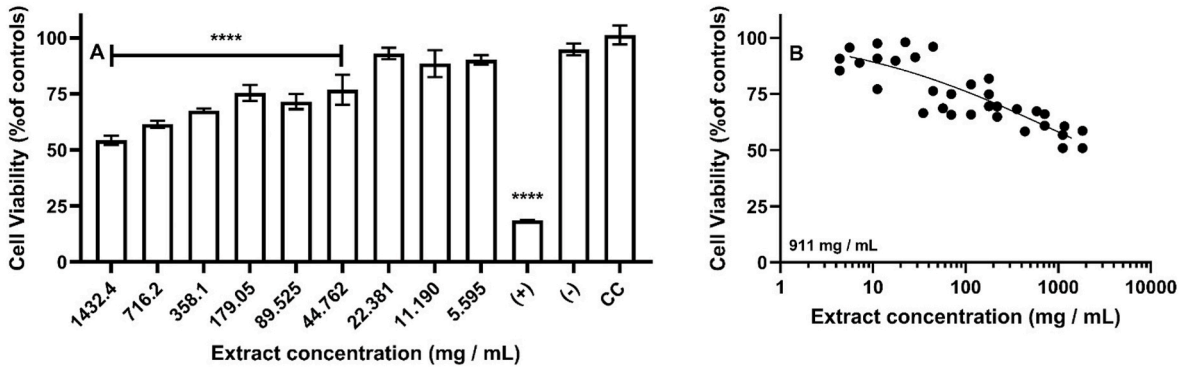

Fig. 6. Cytotoxicity assay of SNSC sample: (a) Cell viability as a function of the extract concentrations. (b) Log-scaled concentration–response curve showing an estimated IC_{50} of 911 mg/mL.

Table 4
Numerical predictions of the risk of failure determined for the Si_3N_4 (Mohr-Coulomb criterion) used as the implant in the second-molar region as a function of the masticatory loading conditions from 50 N up to 400 N.

Mohr-Coulomb Analysis									
Load Direction		50 N	100 N	150 N	200 N	250 N	300 N	350 N	400 N
Normal	90°	0.047	0.095	0.142	0.190	0.237	0.285	0.332	0.380
Occlusal	45°(1)	0.154	0.307	0.461	0.614	0.768	0.921	1.075	1.228
	45°(2)	0.156	0.313	0.469	0.626	0.782	0.939	1.095	1.252
	45°(3)	0.147	0.294	0.441	0.588	0.735	0.882	1.029	1.177
	45°(4)	0.154	0.308	0.461	0.615	0.769	0.923	1.076	1.230

grains of β-Si_3N_4 dispersed in a secondary phase. Good mechanical properties, such as fracture toughness (7.54 ± 0.78 MPa $m^{1/2}$), compressive strength (1497.42 ± 74.06 MPa) and Young's modulus (211.23 ± 63.81 GPa) were found. Moreover, the material was shown non-cytotoxic even at an extract concentration of 1500 mg/mL. The risk of implant failure in critical applications (second-molar) was determined by using a geometric model of a commercial ceramic implant, experimental values, finite element simulations, and the Mohr-Coulomb failure criterion. The analysis indicated the high potential of silicon nitride application since the ceramic implants can be used for masticatory loads of up to 350 N, without risk of failure, within the experimental limits proposed in this study. In the future, different geometries and positions should be studied together with the human jaw to make this model viable for different clinical cases.

CRediT authorship contribution statement

Paula Cruz Mendes Silva: Methodology, Conceptualization. **Pedro Araújo da Costa Ward:** Methodology, Conceptualization. **Patrick Lima Gomes:** Methodology. **Thais Monteiro da Silva:** Methodology. **Flávio Machado de Souza Carvalho:** Methodology. **Daniel Perez Vieira:** Writing – review & editing. **Dolores Ribeiro Ricci Lazar:** Writing – review & editing, Conceptualization. **Claudinei dos Santos:** Writing – review & editing, Conceptualization. **Cecilia Chaves Guedes-Silva:** Writing – review & editing, Project administration, Conceptualization.

Declaration of generative AI and AI-assisted technologies in the writing process

During the preparation of this work, the authors used ChatGPTin order to improve readability and language. After using this tool, the authors reviewed and edited the content as needed and take full responsibility for the content of the publication.

Funding information

The authors acknowledge CNPq (Grants 140942/2023-8, 311119/2017-4) and FAPERJ (Grants E−26/211.212/2021) and COPDE-IPEN (2020.06.IPEN.30) for their financial support.

Declaration of competing interest

The authors declare that they have no known competing financial interests or personal relationships that could have appeared to influence the work reported in this paper.

Appendix A. Supplementary data

Supplementary data to this article can be found online at https://doi.org/10.1016/j.ceramint.2025.12.177.

References

[1] C.C. Guedes-Silva, A.C.D. Rodas, F.M.S. Carvalho, O.Z. Higa, T.S. Ferreira, Silicon nitride with titania, calcia and silica additives for orthopaedic applications, Process. Appl. Ceram. 14 (2020) 63–70, https://doi.org/10.2298/PAC2001063G.
[2] C.C. Guedes-Silva, Bkönig Jr, M.J. Carbonari, M. Yoshimoto, S.A. Allegrini Jr, J. C. Bressiani, Tissue response around silicon nitride implants in rabbits, J. Biomed. Mater. Res. 84 (2008) 337–343, https://doi.org/10.2298/PAC2001063G.
[3] A. A Found, L.R. De Pretto, V. Ussui, N.B. Lima, G.M. De Souza, J.P.B. Machado, R. N. Tango, Z. Freitas, D.R.R. Lazar, Optical coherence tomography (OCT) for the analysis of zirconia crystalline phase transformation, Materialia 30 (2023) 101825, https://doi.org/10.1016/j.mtla.2023.101825.
[4] Z. Badran, X. Struillou, F.J. Hughes, A. Soueidan, A. Hoonaert, M. Ide, Silicon nitride (Si_3N_4) implants: the future of dental implantology? J. Oral Implantol. 43 (2017) 240–244, https://doi.org/10.1563/aaid-joi-D-16-00146.
[5] M. Aparicio-Razo, J.L.J. Mongalo-Váquez, J.A.Y. Ramos, A.H. Navarro-Zárate, V. H. Santos-Enríquez, I.F. Vivanco-Pérez, J.F. Méndez, G.A. Paredes-Juárez, Comparison of material properties for dental implants: titanium, polyetheretherketone, zirconium and silicon nitride, Adv. Mater. Lett. 12 (2022) 1–13, https://doi.org/10.5185/amlett.2022.01168.
[6] X. Chen, K. Shah, S. Dong, L. Peterson, E.C. La Plante, G. Sant, Elucidating the corrosion-related degradation mechanisms of a Ti-6Al-4V dental implant, Dent. Mater. 36 (2020) 431–441, https://doi.org/10.1016/j.dental.2020.01.008.
[7] A. Ouldyerou, H. Mehboob, A. Merdji, L. Aminallah, A. Mehboob, O.M. Mukdadi, Biomechanical analysis of printable functionally graded material (FGM) dental implants for different bone densities, Comput. Biol. Med. 150 (2022) 106111, https://doi.org/10.1016/j.compbiomed.2022.106111.
[8] H.J. Haugen, H. Chen, Is there a better biomaterial for dental implants than titanium? A review and meta-study analysis, J. Funct. Biomater. 13 (2022) 46, https://doi.org/10.3390/jfb13020046.
[9] M.S. Özodogan, M. Gügörmüs, A. Çelik, G. Topates, Silicon nitride ceramic for all-ceramic dental restoration, Dent. Mater. J. 39 (2020) 1080–1086, https://doi.org/10.4012/dmj.2020-134.
[10] X. Du, S.S. Lee, G. Blugan, S.J. Ferguson, Silicon nitride as a biomedical material: an overview, Int. J. Mol. Sci. 23 (2022) 6551, https://doi.org/10.3390/ijms23126551.
[11] C.R. Sona-Filho, F.M. Carvalho, C.C. Guedes-Silva, Mechanical properties and in vitro bioactivity of silicon nitride ceramics with SiO_2, CaO and MgO additions, J. Biomed. Mater. Res. 110 (2022) 507–516, https://doi.org/10.1002/jbm.b.34930.
[12] C.C. Guedes-Silva, A.C.D. Rodas, A.C. Silva, C. Ribeiro, F.M.S. Carvalho, O.Z. Higa, et al., Microstructure, mechanical properties and in vitro biological behavior of silicon nitride ceramics, Mater. Res. 21 (2018) e20180266, https://doi.org/10.1590/1980-5373-MR-2018-0266.
[13] T.J. Webster, A.A. Patel, M.N. Rahaman, B. Sonny Bal, Anti-infective and osteointegration properties of silicon nitride, poly(ether ether ketone), and titanium implants, Acta Biomater. 8 (2012) 4447–4454, https://doi.org/10.1016/j.actbio.2012.07.038.
[14] L. He, N. Huang, D. Lu, P. Sheng, W. Zou, A study on the effects of liquid phase formation temperature and the content of sintering aids on the sintering of silicon nitride ceramics, Crystals 13 (2023) 1114, https://doi.org/10.3390/cryst13071099.
[15] Y. Wu, H. Liu, Y. Zhang, Z. Wu, Q. Chu, Silicon nitride as a potential candidate for dental implants: osteogenic activities and antibacterial properties, J. Mater. Res. 36 (2021) 1866–1882, https://doi.org/10.1557/s43578-021-00249-8.
[16] R. Zhao, R. Yang, P.R. Cooper, Z. Khurshid, A. Shavandi, J. Ratnayake, Bone grafts and substitutes in dentistry: a review of current trends and developments, Molecules 26 (2021) 3007, https://doi.org/10.3390/molecules26103007J.
[17] E. Marin, M. Zanocco, F. Boschetto, M. Santini, W. Zhu, T. Adachi, et al., Silicon nitride laser cladding: a feasible technique to improve the biological response of zirconia, Mater. Des. 191 (2020) 108649, https://doi.org/10.1016/j.matdes.2020.108649.
[18] G. Pezzotti, E. Marin, M. Zanocco, F. Boschetto, W. Zhu, B.J. McEntire, et al., Osteogenic enhancement of zirconia-toughened alumina with silicon nitride and bioglass, Ceramics 2 (2019) 554–567, https://doi.org/10.3390/ceramics2040043.
[19] V. Sharanraj, C. Ramesha, V. Kumar, M. Sadashiva, Finite element analysis of zirconia ceramic biomaterials used in medical dental implants, Interceram. Int. Ceram. Rev. 68 (2019) 24–31, https://doi.org/10.1007/s42411-019-0004-0.
[20] P.A.D.C. Ward, F.A.D.C. Ward, T.M. Ward, C. Santos, R.X.D. Freitas, L.P. Moreira, A strength behavior approach for 3Y-TZP ceramics dental implants based on finite

element simulations, Mater. Res. 26 (2023) e20220110, https://doi.org/10.1590/1980-5373-MR-2022-0110.
[21] P.A.C. Ward, F. Ward, M.F. Rodrigues Pais Alves, C.R. Moreira da Silva, L. P. Moreira, C. Santos, Numerical analysis of the mechanical behavior of ceramic dental implants based on Ce-TZP/Al_2O_3 composite, J. Mech. Behav. Biomed. Mater. 150 (2024) 106335, https://doi.org/10.1016/j.jmbbm.2023.106335.
[22] T. Grippi, S. Béhar-Lafenetre, H. Friedrich, D. Haas, U. Schenderlein, S. Marinel, C. Manière, Finite element simulation for Si_3N_4 heating and sintering, J. Eur. Ceram. Soc. 44 (2024) 116703, https://doi.org/10.1016/j.jeurceramsoc.2024.116703.
[23] L. Wan, Z. Liu, Z. Deng, L. Li, W. Liu, Simulation and experimental research on subsurface damage of silicon nitride grinding, Ceram. Int. 44 (2018) 8290–8296, https://doi.org/10.1016/j.ceramint.2018.02.014.
[24] A.K. Khader, Damage mechanisms in silicon nitride wire-rolling tools: Lab-scale experiments and correlation with finite element modeling, J. Mater. Process. Technol. 210 (2010) 1314–1325, https://doi.org/10.1016/j.jmatprotec.2010.03.021.
[25] Y. Kadin, M. Mazaheri, V. Zolotarevskiy, C. Vieillard, M. Hadfield, Finite elements based approaches for the modelling of radial crack formation upon Vickers indentation in silicon nitride ceramics, J. Eur. Ceram. Soc. 39 (2019) 4011–4022, https://doi.org/10.1016/j.jeurceramsoc.2019.05.058.
[26] A. Neumann, C. Unkel, C. Werry, C.U. Herborn, H.R. Maier, C. Ragoß, K. Jahnke, Prototype of a silicon nitride ceramic-based miniplateosteofixation system for the midface, Otolaryngol. Head Neck Surg. 134 (2006) 923–930, https://doi.org/10.1016/j.otohns.2006.01.022.
[27] P. Zhou, D. Xia, Z. Ni, T. Ou, Y. Wang, H. Zhang, L. Mao, K. Lin, S. Xu, J. Liu, Calcium silicate bioactive ceramics induce osteogenesis through oncostatin M, Bioact. Mater. 6 (2021) 810–822, https://doi.org/10.1016/j.bioactmat.2020.09.018.
[28] A.K. Singh, K. Pramanik, A. Biswas, MgO enables enhanced bioactivity and antimicrobial activity of nanobioglass for bone tissue engineering application, Mater. Technol. 34 (2019) 1–9, https://doi.org/10.1080/10667857.2019.1638636.
[29] L. Fu, Y. Xiong, G. Carlsson, M. Palmer, S. Örn, W. Zhu, X. Weng, H. Engqvist, W. Xia, Biodegradable Si_3N_4bioceramic sintered with Sr, Mg and Si for spinal fusion: surface characterization and biological evaluation, Appl. Mater. Today 12 (2018) 260–275, https://doi.org/10.1016/j.apmt.2018.06.002.
[30] P. Chantikul, G.R. Anstis, B.R. Lawn, D.B. Marshall, A critical evaluation of indentation techniques for measuring fracture toughness: II, Strength method, J. Am. Ceram. Soc. 64 (1981) 539–543, https://doi.org/10.1111/j.1151-2916.1981.tb10321.x.
[31] G.R. Anstis, P. Chantikul, B.R. Lawn, D.B. Marshall, A critical evaluation of indentation techniques for measuring fracture toughness: i, direct crack measurements, J. Am. Ceram. Soc. 64 (1981) 533–542, https://doi.org/10.1111/J.1151-2916.1981.TB10320.X.
[32] W.C. Oliver, G.M. Pharr, An improved technique for determining hardness and elastic modulus using load and displacement sensing indentation experiments, J. Mater. Res. 7 (1992) 1564–1583, https://doi.org/10.1557/JMR.1992.1564.
[33] W.C. Oliver, G.M. Pharr, Measurement of hardness and elastic modulus by instrumented indentation: advances in understanding and refinements to methodology, J. Mater. Res. 19 (2004) 3–20, https://doi.org/10.1557/jmr.2004.19.1.3.
[34] Straumann, Straumann product catalogue. https://www.straumann.com/content/dam/media-center/straumann/en/documents/catalog/product-catalog/452.201-en_low.pdf, 2024. (Accessed 6 November 2024).
[35] T. Schneider, Y. Hu, X. Gao, J. Dumas, D. Zorin, D. Panozzo, A large-scale comparison of tetrahedral and hexahedral elements for solving elliptic PDEs with the finite element method, TOG41 (2022) 1–14, https://doi.org/10.1145/3508372.
[36] O. Lukinova, Mechanical and elastic properties of new silicon nitride ceramics produced by cold isostatic pressing and free sintering, Ceram. Int. 41 (2015) 13716–13720, https://doi.org/10.1016/j.ceramint.2015.08.026.
[37] J.F. Labuz, A. Zang, in: Mohr–Coulomb failure criterion, The ISRM Suggested Methods for Rock Characterization, Testing and Monitoring: 2007-2014, Springer International Publishing, Cham, 2014, pp. 227–233, https://doi.org/10.1007/s00603-012-0281-7.
[38] P. Marcián, L. Borák, T. Zikmund, L. Horáčková, J. Kaiser, M. Joukal, J. Wolff, On the limits of finite element models created from (micro)CT datasets and used in studies of bone–implant-related biomechanical problems, J. Mech. Behav. Biomed. Mater. 117 (2021) 104393, https://doi.org/10.1016/j.jmbbm.2021.104393.
[39] S. Hampshire, Structure and bulk properties of silicon nitride, in: B.S. Bal, B. J. McEntire, G. Pezzotti (Eds.), Silicon Nitride Bioceramics, Springer, Cham, 2024, https://doi.org/10.1007/978-3-031-67047-3_2.
[40] [40a] M. Komaki Matsuura, T. Ohji, T. Takahashi, M. Iijima, J. Tatami, Effects of rare-earth oxides on grain boundary strength of silicon nitride ceramics, J. Eur. Ceram. Soc. 44 (2024) 116672, https://doi.org/10.1016/j.jeurceramsoc.2024.116672B;
[40b] S. Bal, M.N. Rahaman, Orthopedic applications of silicon nitride ceramics, Acta Biomater. 8 (2012) 2889–2898, https://doi.org/10.1016/j.actbio.2012.04.031.
[41] X. Zeng, C.S. Sipaut, N.M. Ismail, Y. Liu, Y. Farm, J. He, Mechanical properties and biological activity of 3D printed silicon nitride materials, Ceram. Int. 50 (2024) 16704–16713, https://doi.org/10.1016/j.ceramint.2024.02.041.
[42] H. Mohammadi, S. Beddu, M. Petrů, M. Sepantafar, M. Ebadi, B.K. Yap, et al., Advances in silicon nitride ceramic biomaterials for dental applications – a review, J. Mater. Res. Technol. 28 (2024) 2778–2791, https://doi.org/10.1016/j.jmrt.2023.12.186.
[43] M.C. Sobieraj, C.M. Rimnac, Fracture, fatigue, and notch behavior of PEEK, in: PEEK Biomaterials Handbook, Elsevier Inc., 2019, pp. 67–82, https://doi.org/10.1016/B978-0-12-812524-3.00005-3.
[44] R.B. Heimann, Silicon nitride ceramics: structure, synthesis, properties, and biomedical applications, Mater 16 (2023) 5142–5158, https://doi.org/10.3390/ma16145142.
[45] T. Hanawa, Zirconia versus titanium in dentistry: a review, Dent. Mater. J. 39 (2020) 24–36, https://doi.org/10.4012/dmj.2019-172.
[46] ICRP, Basic anatomical and physiological data for use in radiological protection: reference values. ICRP Publication 89, Ann. ICRP 32 (3–4) (2002) 1–277.
[47] J.P. Geng, K.B. Tan, G.R. Liu, Application of finite element analysis in implant dentistry: a review of the literature, J. Prosthet. Dent 85 (2001) 585–598, https://doi.org/10.1067/mpr.2001.115251.
[48] L.C. Has, R. Orbak, Effect of bone quality, implant length, and loading timing on stress transmission in the posterior mandible: a finite element analysis, Bioengineering 12 (2025) 888, https://doi.org/10.3390/bioengineering12080888.
[49] S.M. Choi, E.J. Park, J.Y. Lee, Y.C. Jeon, M.J. Yun, Comparative finite element analysis of mandibular posterior zirconia and titanium implant-supported prostheses, J. Adv. Prosthodont. 13 (2021) 225–234, https://doi.org/10.4047/jap.2021.13.6.396.
[50] V. dos Santos Marsico, R.B. Lehmann, C.A. de Assis Claro, M. Amaral, R.P. Vitti, A. C.C. Neves, L.R. da Silva Concilio, Three-dimensional finite element analysis of occlusal splint and implant connection on stress distribution in implant-supported fixed dental prosthesis and peri-implantal bone, Mater. Sci. Eng. C 80 (2017) 141–148, https://doi.org/10.1016/j.msec.2017.05.071.